Rheology of Polymer Melts in High Shear Rate

HIDEROH TAKAHASHI, TAKAAKI MATSUOKA, and TOSHIO KURAUCHI, *Toyota Central Research and Development Laboratories, Inc., Nagakute-cho, Aichi-gun, Aichi-ken, 480-11, Japan*

Synopsis

Little is known of the rheology of polymer melts in the high shear rate up to 10^6 s^{-1} or more. A specially designed high-shear-rate rheometer was developed, by which the rheology of polymer melts for shear rates up to 10^8 s^{-1} can be investigated. Two non-Newtonian regions and a transition or the second Newtonian region were observed in the wide range of shear rates up to 10^7 s^{-1}. The observed flow curves for various polymer melts are classified into three typical patterns. One is the flow curve typically shown of high-density polyethylene in which a clear second Newtonian region appears after the first non-Newtonian region. The second is the typical flow curve of polystyrene in which a "transition region" appears instead of the second non-Newtonian region. The third is the flow curve shown of acrylonitrile-styrene copolymer, which exhibits behavior between the two types. A generalized flow curve is proposed to explain the observed flow behaviors of various polymers over a wide range of shear rates. The flow behavior in high shear rate results from high orientation and scission of polymer molecules.

INTRODUCTION

It is well known that polymer melts behave as Newtonian fluids with shear rates below about 1 s^{-1}, and as non-Newtonian fluids at higher shear rates. In injection molding, the shear rate up to 10^6 s^{-1} may be attained under high pressure. This exceeds the limit of most conventional rheometers. Consequently, very little is known of the rheology of polymer melts at shear rates from 10^4 to 10^6 s^{-1}. Recent trends toward a high-speed injection molding makes it very important to study rheology in this range.[1] The rheology of polymer melts under such higher shear rate has not been reported. Then it would therefore be very interesting to study the rheology of polymer melts in such high shear rates as an aid for the development of new polymer processing methods.

A specially designed high-shear-rate rheometer has been developed, by which the rheology of polymer melts for shear rates up to 10^8 s^{-1} can be investigated. Viscosity-shear rate curves of seven kinds of polymer melts were measured at shear rates up to 10^7 s^{-1} with this new high-shear-rate rheometer. Flow characteristics were investigated through the characterization of extrudates and the observation of flow behaviors.

EXPERIMENTAL

Figure 1 shows an outline of the specially designed capillary rheometer. The high-shear-rate rheometer is of a capillary type, and consists of a die (nozzle) and a specially designed injection unit. The injection unit is composed of a heated cylinder, a reciprocal plunger, and a hydraulic power

Journal of Applied Polymer Science, Vol. 30, 4669–4684 (1985)
 CCC 0021-8995/85/124669-16$04.00

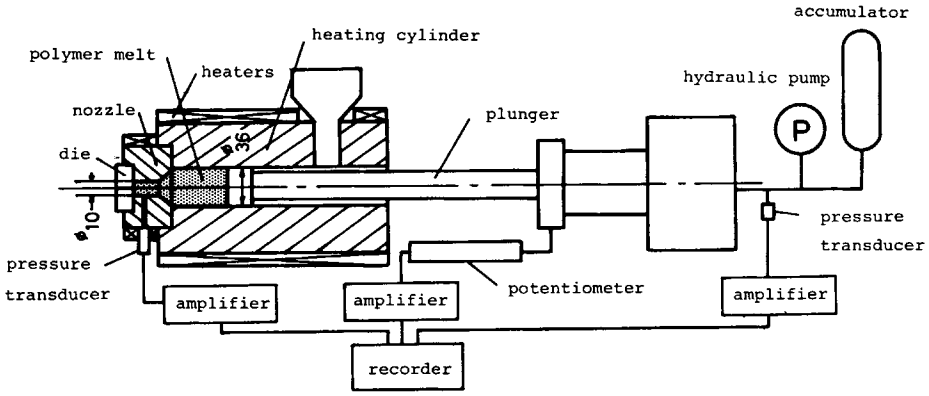

Fig. 1. Outline of the specially designed capillary rheometer.

unit. To achieve the high shear rates of 10^8 s^{-1}, the hydraulic power unit is equipped with two accumulators and a shrinkage fitted barrel is used as a heating cylinder to maintain the high pressure of 7000 kgf/cm^2 (6.86×10^2 MPa). Five separate heaters are arranged along the barrel and the nozzle, and temperature of all parts is controlled at the same value. The speed of the injection plunger can be varied widely by adjusting three kinds of flow control valves. Dies with various sizes of capillaries were used for this study. Capillaries of the length of 2.5, 5, 10, 15, and 20 mm and capillaries of the diameter of 0.4, 0.5, 0.6, 0.75, and 1.0 mm were available. The capillary of 0.5 mm diameter and 10 mm length was used for most of the study described in this paper. Some of the data were obtained using a conventional capillary rheometer (Shimazu, Autograph) by which flow curves in a low shear rate range up to 10^4 s^{-1} can be obtained.

The nozzle pressure was measured at the entrance to the die by the use of a pressure transducer (Sensotec, Pressure Transducer Type T/2941). The injection pressure was also measured at the inlet to the hydraulic cylinder with another pressure transducer (Toyoda Machine Works, Type PMS-8M). The position and the velocity of the plunger were determined by a linear potentiometer. The pressures and the velocity were recorded against the plunger position on an X-Y recorder.

The shear stress at the capillary wall τ_w is given by the equation

$$\tau_w = \frac{\Delta P R}{2L} \tag{1}$$

where ΔP is a pressure drop along the die and R and L are the radius and the length of the capillary, respectively.

The apparent shear rate, $\dot{\gamma}_a$, is given by the equation

$$\dot{\gamma}_a = \frac{4Q}{\pi R^3} \tag{2}$$

where Q is the volumetric flow rate, obtained from the velocity of the

plunger. The apparent viscosity η_a is defined as

$$\eta_a = \frac{\tau_w}{\dot{\gamma}_a} \tag{3}$$

The "backflow leak" between the injection cylinder and the plunger was estimated by measuring the displacement of the plunger under various pressure settings with a closing plug in the barrel in place of a die. No backflow leakage was observed for polystyrene melt under pressures less than 3700 kgf/cm^2 (3.63 $\times$ 10^2 MPa) and little leakage (approximately 0.02 cm^3/s) was observed under a pressure of 5000 kgf/cm^2 (4.90 $\times$ 10^2 MPa). This value corresponds to 0.04% of the volumetric flow rate determined at the same pressure. Similar results are obtained for the other polymers. Therefore, the influence of flow leakage can be neglected in this experiment. In the low-shear-rate region, extrudate temperatures were measured by plunging a sheathed thermocouple with an outer diameter of 0.5 mm into the extrudate immediately after it emerged from the die. In the high-shear-rate region, the temperature of the extrudate was measured at the exit of the die by the use of an infrared thermal video system (Nippon Avionics, TVS-4500). For observation of the flow behavior of the extrudates, high-speed motion pictures were taken.

Seven kinds of commercially available polymers were investigated in the present study. These materials were polystyrene (Mitsui Thoatsu Chemicals, Torporex GP 550-51), high-density polyethylene (Mitsui Petrochemical, Hizex 2100J), ultra-high-molecular-weight polyethylene (Mitsui Petrochemical, Hizex Million M240), acrylonitrile-styrene copolymer (Mitsubishi Monsant Chemical, Sanrex SAN-H), polycarbonate (Mitsubishi Gas Chemical, Iupilon S-3000), polypropylene (Chisso, PP K1016), and polyamide-6,6 (Asahi Chemical, Leona 1300S).

The molecular weight distribution of the extrudates, which were extruded in air or liquid nitrogen, were measured by the use of gel permeation chromatography (Waters Associates). Tetrahydrofuran was used as the solvent for polystyrene (PS), acrylonitrile-styrene copolymer (SAN), and polycarbonate (PC). *o*-Dichlorobenzene was used for high-density polyethylene (HDPE) and polypropylene (PP) and *m*-crezol was used for polyamide-6,6 (PA-6,6).

Fourier transform infrared spectroscopy (FT-IR; JEOL, Ltd. JIR-100) was used to obtain the infrared spectra of the extrudates. Films of extrudates for infrared measurements were prepared by solvent casting after the extrudate dissolved in chloroform. Reference films were prepared from the pellets in the same manner. To obtain the infrared spectrum for thermally degraded material, pellets were heated to 230°C for 6 h in air and the film prepared.

RESULTS

The apparent viscosities of PS melt are plotted against apparent shear rates in Figure 2. The viscosities at shear rates less than 10^4 s^{-1} were measured with a conventional capillary rheometer and the viscosities above

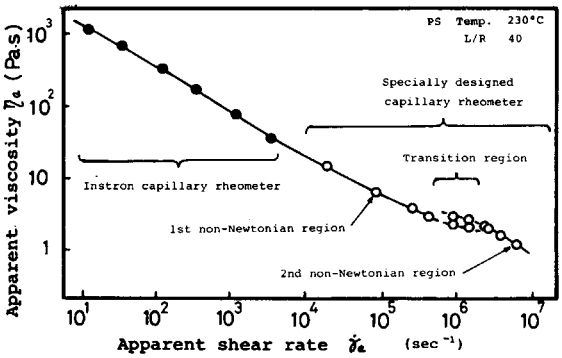

Fig. 2. Plot of apparent viscosity η_a vs. apparent shear rate $\dot{\gamma}_a$ for PS.

10^4 s^{-1} were measured with the specially designed capillary rheometer. The flow curves obtained separately connect smoothly with one another. An unexpected transition region were observed in the high-shear-rate region above 5×10^5 s^{-1}. In the transition region, dual values of the apparent viscosity were obtained at one shear rate. Such dual values in viscosity were sometimes observed even in one extrusion stroke; the lower value occurred at the earlier stage of the extrusion, and it fit the extrapolation of the first non-Newtonian curve, as shown in Figure 2. The higher value occurred at the later stage of the extrusion and it fit the extrapolation of the second non-Newtonian curve.

Figure 3 shows a plot of extrudate temperature versus apparent shear rates for PS melts. The temperature rise at the apparent shear rate of 3×10^6 s^{-1} was about 50°C. This value was about one-half of the value calculated on the assumption that the energy of the extrusion was fully converted to heat (adiabatically). An increase in temperature should decrease the viscosity. However, the viscosity in the transition and the second non-Newtonian region is higher than extrapolated value of the first non-Newtonian curve.

Flow curves in the high-shear-rate region of PS at various stock temperature are shown in Figure 4. The temperature dependence of the viscosity

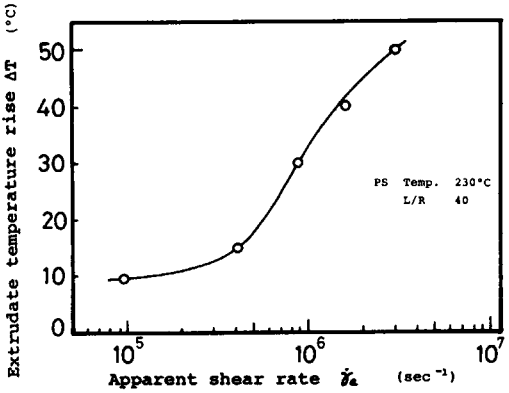

Fig. 3. Plot of extrudate temperature rise ΔT vs. apparent shear rate $\dot{\gamma}_a$ for PS.

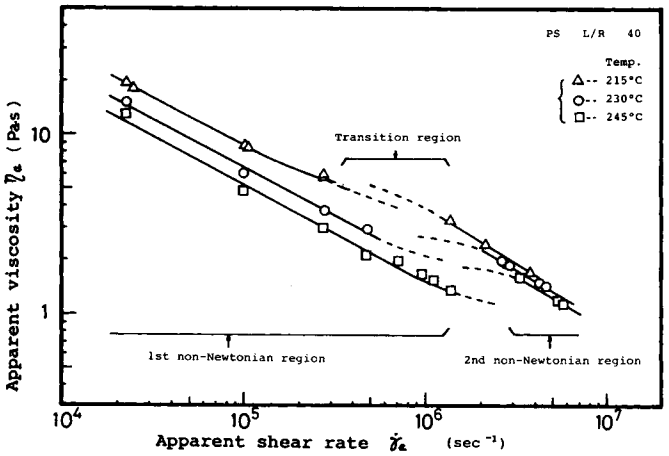

Fig. 4. Flow curves in high-shear-rate region for PS at various temperature.

is small, especially in the second non-Newtonian region in comparison with the temperature dependence of the viscosity in the first non-Newtonian region. These results suggest the occurrence of an unknown phenomenon, for example, extremely high orientation, scission, and restriction of the movement of the polymer chain under these very high shear rates and pressures.

Figure 5 shows the flow curve of the previously extruded PS at a shear rate of 3.2×10^6 s^{-1}, in which the flow curve of the virgin PS is also replotted. It is clear that there is little difference between two flow curves.

The apparent viscosities of HDPE melt are plotted against the apparent shear rates in Figure 6. A second Newtonian region, in which the apparent viscosity is constant with shear rate, was clearly observed in the high-shear-rate region ($>3 \times 10^6$ s^{-1}). Flow curves in the high-shear-rate region at various temperature are shown for HDPE and ultra-high-molecular-weight polyethylene (UHMWPE) in Figure 7. The temperature dependence ob-

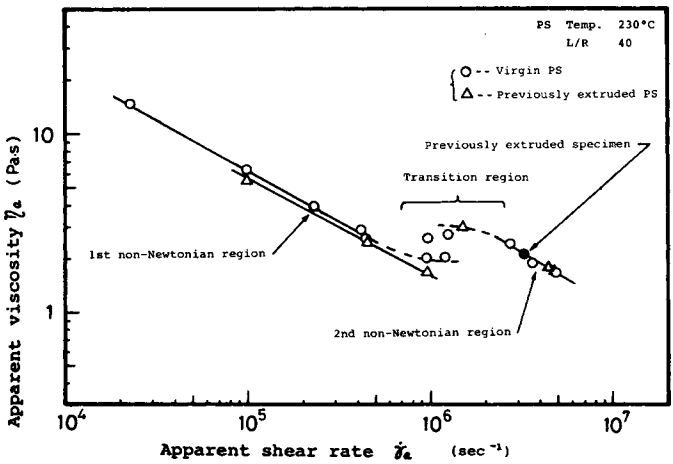

Fig. 5. Flow curves of previously extruded PS and virgin PS.

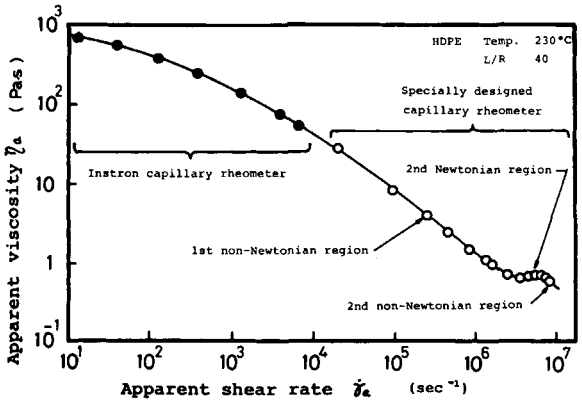

Fig. 6. Plot of apparent viscosity η_a vs. apparent shear rate $\dot{\gamma}_a$ for HDPE.

served for the viscosity of HDPE is less than for PS at shear rate above 10^4 s^{-1}. A second Newtonian region was also clearly observed in the flow curve of UHMWPE. The apparent viscosity of UHMWPE is nearly the same as that of HDPE in the second non-Newtonian region.

The apparent viscosities of SAN and PC are plotted against apparent shear rate in Figure 8. The flow characteristics of SAN is similar to that of PS. Again, a transition region was observed in the high-shear-rate region. The apparent viscosity becomes large at apparent shear rates of about 3×10^6 s^{-1}, above which the second non-Newtonian region appears. The viscosity-temperature dependence in the second non-Newtonian region is not so marked in comparison with that in the first non-Newtonian region.

A flow curve observed up to the shear rate of 1×10^6 s^{-1} for PC is also shown in Figure 8. Only the first non-Newtonian region was observed. Since the viscosity of PC is very large at a temperature of 280°C, the flow curve could not be observed at shear rates greater than 1×10^6 s^{-1}.

The apparent viscosities of PP and PA-6,6 are plotted against the apparent shear rate in Figure 9. The flow characteristic of PP was similar to that of

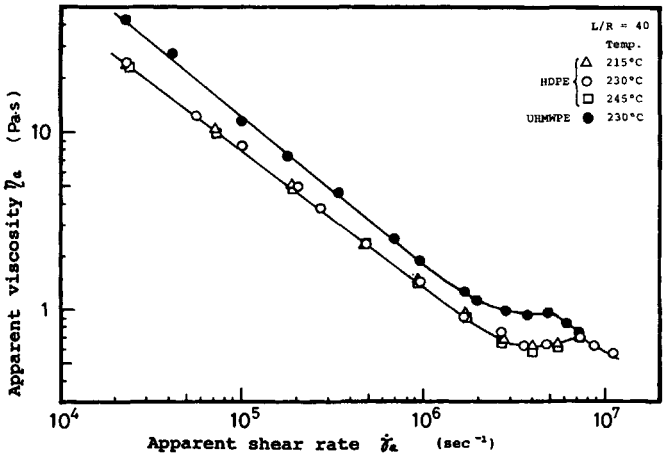

Fig. 7. Flow curves in the high-shear-rate region for HDPE and UHMWPE.

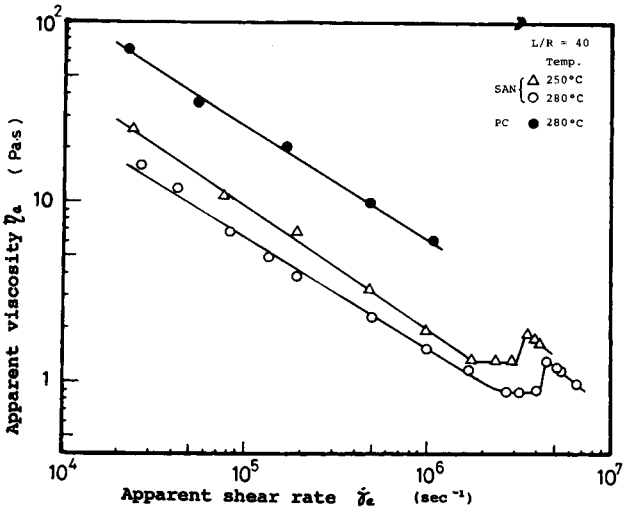

Fig. 8. Flow curves in the high-shear-rate region for SAN and PC.

HDPE except PP exhibited a larger temperature dependence. The second Newtonian region was clearly observed, but the second non-Newtonian region was not evident up to shear rates of 6×10^6 s^{-1}.

The flow characteristics of PA-6,6 at 280°C were similar to that of SAN. A peak appeared in the flow curve at a shear rate of 3.5×10^6 s^{-1}. The peak, however, disappeared in flow curves observed at 290 and 300°C, and a second Newtonian region was observed similarly to that for HDPE. Figure 10 shows the flow curves of PP obtained by the use of two kinds of the capillaries that had the same L/R ratio but different radii. It is observed that the apparent viscosity is independent of the capillary radius. Similar results were obtained for the other polymers. From these observations, the validity of the no slip assumption[2] is confirmed.

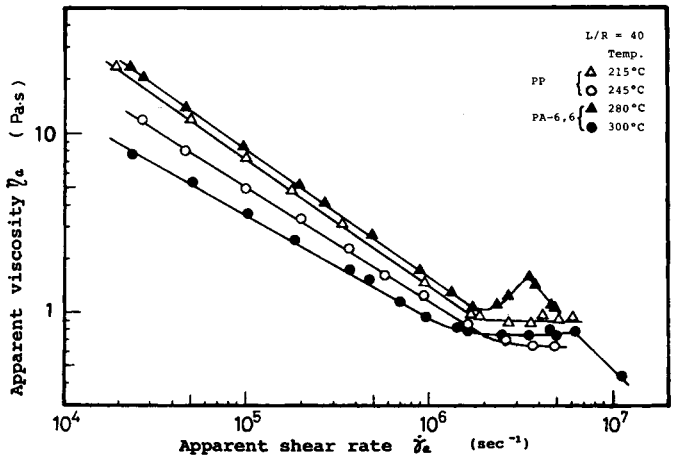

Fig. 9. Flow curves in the high-shear-rate region for PP and PA-6,6.

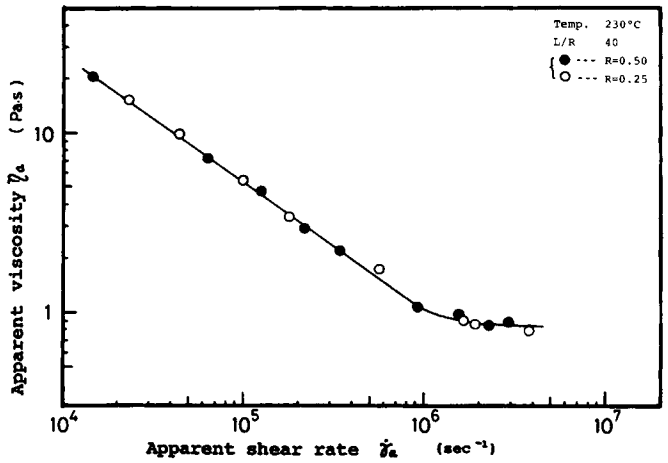

Fig. 10. Flow curves of PP obtained by the use of two kinds of capillaries that have the same L/R ratio but different radii.

Reynold's number N_{Re}', for a power law fluid[3] and velocity head ratio H_v are defined by following equations.

$$N_{Re}' = \frac{D^n V^{2-n} \rho}{gK8^{n-1}(3n + 1/4n)^n} \tag{4}$$

where D is a capillary diameter, V average velocity, ρ density, g gravitational acceleration, and K and n the power law constants.

$$H_v = \frac{(\rho V^2/2g)}{\Delta P} \tag{5}$$

Figure 11 shows the calculated N_{Re}' and H_v for PS in the high-shear-rate region.

The Reynold's number is about 100 at the highest shear rates in this experiment and because the flow might be considered laminar. The highest

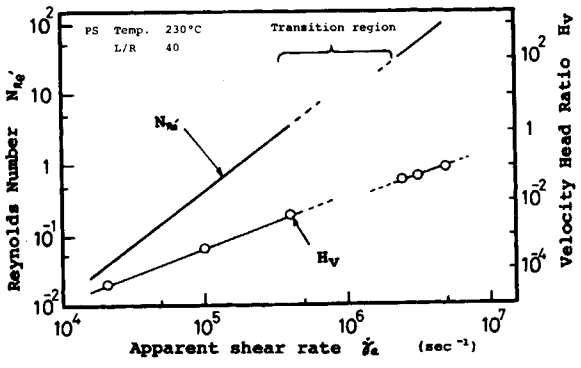

Fig. 11. Reynold's number for a power law fluid N_{Re}' and velocity head ratio H_v in the high-shear-rate region for PS.

velocity head is about 0.1. So, the error in calculation of the viscosity due to the velocity head is considered to be negligible. Similar results were obtained for the other polymers. From these results, it is considered that the observed flow curves give the inherent flow characteristics for laminar flow of the polymer melts.

The weight-average molecular weights $\overline{M}_w$ of the extrudates are plotted against shear rate for PS, HDPE, SAN, and PC in Figures 12 and 13, respectively. In Figure 12, the molecular weights for two kinds of PS are plotted. One is obtained for once extruded PS, and the other is for twice-extruded PS in which the material was first extruded at a constant shear rate of 3.2×10^6 s^{-1} and sequentially extruded at the various shear rates indicated. The previously extruded specimen had the molecular weight of 1.8×10^5, as shown in Figure 12 by the solid circular dot. Little change in the molecular weight of the once-extruded PS was observed for shear rates up to 10^5 s^{-1}. It decreased gradually with increases in the shear rate above 5×10^5 s^{-1}. However, the molecular weight increases sharply and then decreases in the transition region, as shown in Figures 2 and 4.

The molecular weight of the twice-extruded PS decreases similarly to the once-extruded PS with an increase in the shear rate, except in the transition region, where the molecular weight rises slightly and then decreases.

Infrared absorbance difference spectra obtained by subtracting the reference spectrum from the spectrum of the PS extruded in air or that of the thermally degraded PS are shown in Figures 14 and 15.

Two narrow bands are observed in the difference spectra of the PS extrudates at 1630 and 1685 cm^{-1}. The band at 1630 cm^{-1} is not observed for thermally degraded PS. The primary oxidative component during thermal oxidation in air has an absorption at 1685 cm^{-1}.[4] The band at 1630 cm^{-1} can be assigned to a carbon double-bond vibration. This band is observed in the spectrum of the mechanically degraded PS.[4,5] The stronger absorption at 1630 cm^{-1} is observed in the difference spectrum of the PS extrudate extruded at higher shear rates.

These results suggest that both mechanical scission and recombination of molecules occur in the transition region and that polymer scission mainly occurs in the second non-Newtonian region.

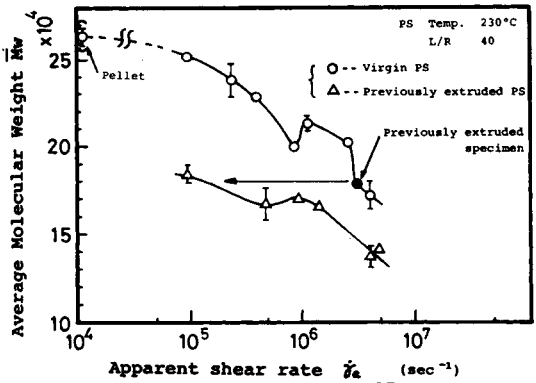

Fig. 12. Weight-average molecular weight $\overline{M}_w$ of the extruded PS.

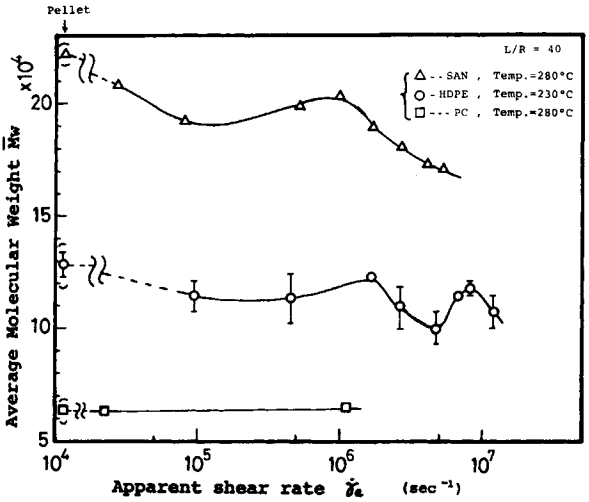

Fig. 13. Weight-average molecular weight $\bar{M}_w$ of extruded SAN, HDPE, and PC.

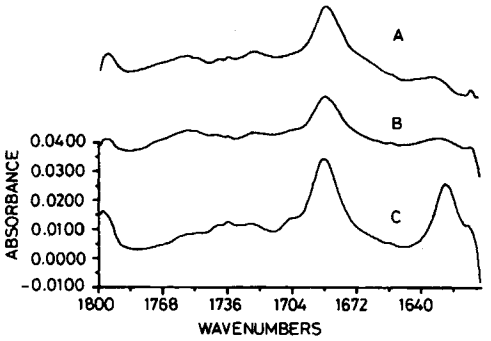

Fig. 14. Infrared absorbance difference spectrum obtained by subtracting the reference spectrum from the spectrum of the PS extruded in air (temperature = 230°C, $L/R = 40$). (A) $\dot{\gamma}_a = 1.0 \times 10^5\ s^{-1}$. (B) $\dot{\gamma}_a = 1.2 \times 10^6\ s^{-1}$. (C) $\dot{\gamma}_a = 4.2 \times 10^6\ s^{-1}$.

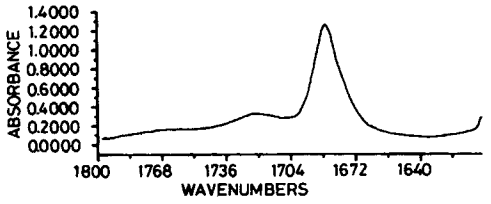

Fig. 15. Infrared absorbance difference spectrum obtained by subtracting the reference spectrum from the spectrum of the thermally degraded PS at 230°C for 6 h.

The molecular weight distributions for the once-extruded PS at various shear rates are shown in Figure 16. Preferential scission of the larger molecules seems to occur mainly under high shear rates.

Figure 13 gives the change of the molecular weight for HDPE, SAN, and PC extrudates. Little change in the molecular weight of HDPE was observed up to 2×10^6 s^{-1}, and above this shear rate, the molecular weight changed in a complicated way. In the high shear rate above 7×10^6 s^{-1}, where the second non-Newtonian region appears, as shown in Figure 6, the molecular weight of HDPE seems to gradually decrease.

No change of the molecular weights of SAN extrudates was observed in the first non-Newtonian region, and the molecular weight decreased with an increase in shear rate in the second Newtonian and the second non-Newtonian regions.

The molecular weight distributions of the SAN extrudates at various shear rates are shown in Figure 17. It is obvious from this figure that the scission of the higher molecules occurs mainly under the high shear, similarly to the PS extrudates.

Little change in molecular weight was observed for PC, whose flow curve was observed only in the first non-Newtonian region in this experiment, as shown in Figure 8.

Extruding behavior from the capillary were observed with a high-speed motion camera. In the first non-Newtonian region (up to a shear rate of 5×10^5 s^{-1}), the extrudate was continuous for PS; in the transition and the second non-Newtonian regions, an intermitted discontinuity of the extrudate was observed, as shown in Figure 18. It is clear that HDPE during extrusion in the second Newtonian and the second non-Newtonian regions is experiencing a partial "atomization," as shown in Figure 18. From Figure 18, the length of the discontinuous extrudate is calculated to be about 50 mm and the extruding velocity is about 300 m/s. Hence, the frequency of the oscillating flow is about 6×10^3 Hz. This oscillating flow seems to be made by the oscillation of the pressure in the capillary, which is either induced by the polymer scission or else induces the polymer scission. Further study, however, is needed to clarify the mechanism of this flow be-

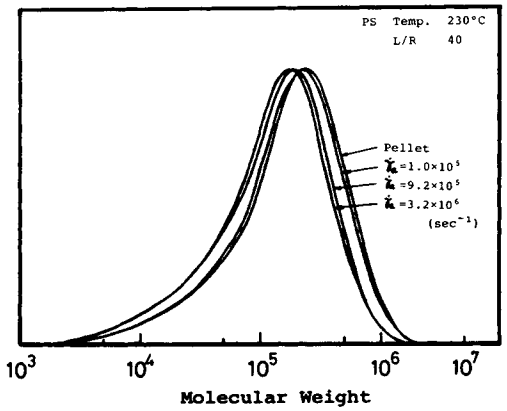

Fig. 16. Molecular weight distributions of PS extrudates.

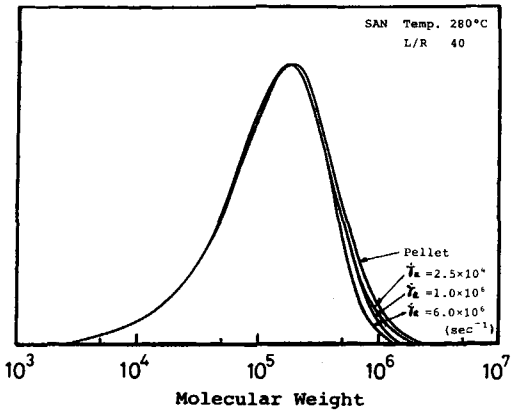

Fig. 17. Molecular weight distributions of SAN extrudates.

havior. It is clear that the intermittent discontinuity and partial atomization of polymers in the region of very high shear rate and the polymer scission also occur under such flow conditions.

DISCUSSION

The flow characteristics of polymer melts obtained in this experiment can be summarized as follows. The observed flow curves for various polymer melts are classified into three typical patterns, as shown in Figure 19. Type

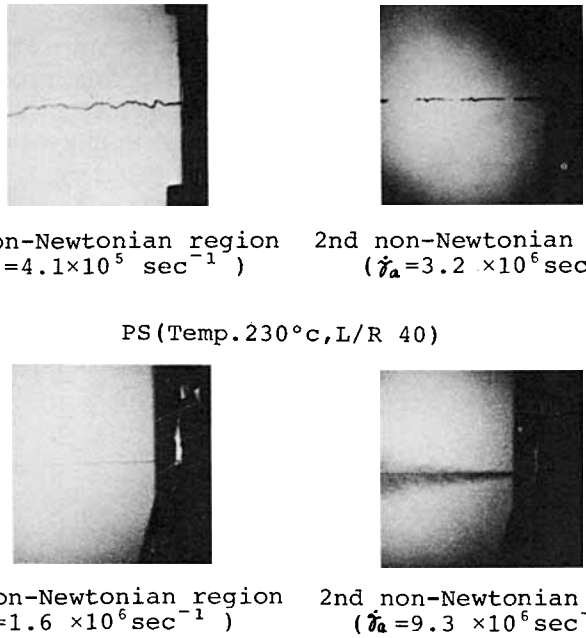

Fig. 18. High-speed motion picture photographs of the extruding behavior out of the capillary (PS and HDPE).

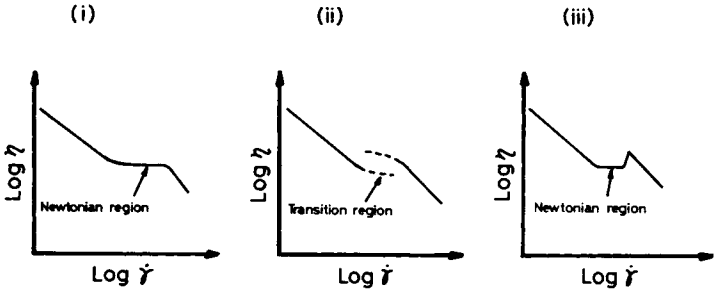

Fig. 19. Three typical patterns of observed flow curves.

(i) is the flow curve typically exhibited by HDPE in which a second Newtonian region clearly appears after the first non-Newtonian region. The flow curves of UHMWPE and PP also fall within this type. Type (ii) is the flow curve shown typically in PS in which a "transition region" appears instead of the second Newtonian region. Type (iii) is the flow curve typically exhibited by SAN and PA-6,6, which falls between these two types. The shape of flow curves exhibited at high shear rate seems to depend on the interaction between molecules, since the flow curves of the polymer melts with small side chains on molecules exhibit type (i) behavior and that of polymer melts with large side chains exhibit type (ii) behavior.

The molecular weights of such polymers as PS and SAN with strong intermolecular interaction decrease when exposed to shear rates beyond the end of the first non-Newtonian region. On the other hand, very little change in molecular weight was observed for HDPE with a weak molecular interaction, even under high shear rates of the second Newtonian region. However, a tendency for the molecular weight to decrease appears at the beginning of the second non-Newtonian region. As shown in Figure 5, the flow curve of previously extruded PS with the molecular weight of 1.8×10^5 is identical to that of virgin PS with a molecular weight of 2.6×10^5. It is thought that the influence of such a molecular weight difference upon the viscosity at very high shear rates should be small. It has been reported that the viscosity dependence on molecular weight decreases with an increase in shear rate, when observed by a conventional rheometer.[6] The small dependence of viscosity on molecular weight at high shear rates is confirmed by comparing the flow curves for HDPE and UHMWPE shown in Figure 7. These polymers had about an order of magnitude difference in their molecular weights.

From the results reported here, a generalized flow curve for polymer melts is proposed, as shown schematically in Figure 20 for a wide range of shear rates. The viscosity in the first non-Newtonian region depends on the creation of entanglements and disengagement. In this region, the viscosity decreases with increases in shear rate, because the entanglement density is reduced as the shear rate increases.[7] In the second Newtonian region, the viscosity is constant because in this region, all the entanglements vanish and the viscosity depends only on the friction of the highly oriented molecules. The flow curve up to the shear rate of the second Newtonian region

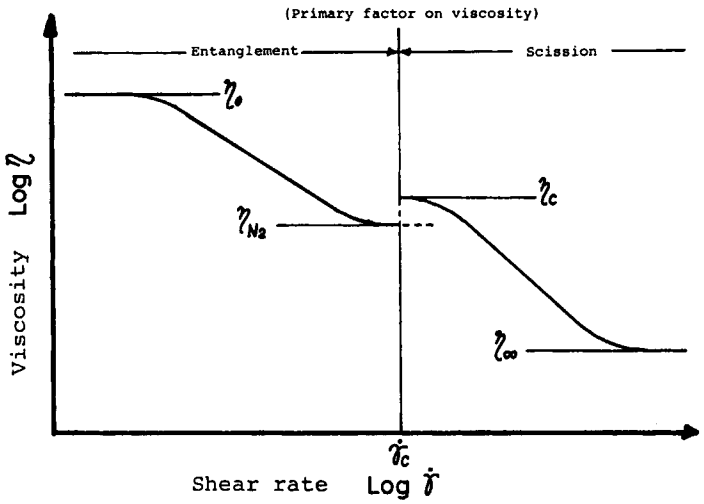

Fig. 20. An extended flow curve for polymer melts in the wide shear rate range.

is given by Soong and Shen[7] as

$$\eta(\dot{\gamma}) = \eta_{N_2} + \frac{\eta_0 - \eta_{N_2}}{1 + (k_1/k_c)(\lambda\dot{\gamma})^m} \tag{6}$$

where $\eta(\dot{\gamma})$ is the viscosity at shear rate $\dot{\gamma}$, η_0 is the zero shear rate viscosity, k_1 and k_c are the entanglement loss and creation rate constants, respectively, λ is a characteristic molecular time constant, m is a constant, and η_{N_2} is the viscosity in the second Newtonian region. Equation (6) shows the good agreement with the observed flow curves reported here.

In the second Newtonian or the transition region, the flow behaviors of polymer melts were found in this study to be complicated. The following equation is, however, proposed to explain the flow behaviors.

$$\eta(\dot{\gamma}) = \eta\infty + \frac{\eta_c - \eta\infty}{1 + (k_s/k_r)[\mu(\dot{\gamma} - \dot{\gamma}_c)]^n} \tag{7}$$

where $\eta\infty$ is the limiting value, which depends on the friction of the smallest molecules obtained by mechanical scission of the polymer, η_c is the viscosity at the critical shear rate $\dot{\gamma}_c$, which is observed in the second Newtonian or transition region, k_s and k_r are the polymer scission and recombination rate constants, respectively, μ is a characteristic molecular time constant, and n is a constant.

As shown in Figure 8, the flow curve of the SAN melt has the second Newtonian region where the viscosity is constant against $\dot{\gamma}$, and the critical phenomenon in the viscosity appears at the critical value of shear rate $\dot{\gamma}_c$. With increases in the melt temperature, $\dot{\gamma}_c$ shifts to higher shear rates. It is thought that this increase in $\dot{\gamma}_c$ may be due to a decrease in the friction between molecules, because the free volume of the melt increases with temperature. That is, $\dot{\gamma}_c$ may depend on the kind of polymer, its free volume,

and the strength of a principal chain. As shown in Figure 9, the flow curve of PA-6,6 melts at 280°C have a critical viscosity η_c, but at 290 and 300°C the peak in η_c is not observed and η_c may become equal to η_{N_2} in eq. (6). The disappearance of the critical phenomenon in the viscosity is due to equal probabilities of molecular scission and recombination or due only to friction of highly oriented molecules without entanglements. The flow curve of the PS melt exhibited no second Newtonian region and has, substitutionally, the transition region in which dual values at one shear rate are observed. In the PS melt, the first and second non-Newtonian regions overlap, so the transition region may be unstable. As a result, the phenomenon of dual values for the viscosity may appear in the transition region.

The average stress applied to a chain at a shear rate of 1×10^6 s^{-1} is estimated to be about one-hundredth of the strength of the principal chain. Molecular scission may occur due to the combined effect of large stresses applied uniformly to a chain and the catalytic effect of dissolved oxygen in the polymer melt. The critical viscosity η_c cannot be estimated because the phenomenon is very complicated. However, that $\eta_c - \eta_{N_2} \geq 0$ is supported in the experiments.

Viscosity depends mainly on polymer scission in the second non-Newtonian region, and therefore the temperature dependence of the viscosity is less in this region than that in the first non-Newtonian region, where the viscosity depends on entanglement density.

It is concluded that eq. (7), based on the proposed generalized flow curve, explains well the observed flow behavior of various polymers in regions of high shear rate.

CONCLUSIONS

The flow characteristics of polymer melts were measured at shear rates up to 10^7 s^{-1} by the use of a specially designed capillary rheometer.

Two non-Newtonian regions and a transition or second Newtonian region were observed in the wide range of the shear rate up to 10^7 s^{-1}. The observed flow curves for various polymer melts are classified into three typical patterns. One is the flow curve observed typically for HDPE in which a clear second Newtonian region appears after the first non-Newtonian region. The flow curves of UHMWPE and PP belong to this type. The second is the flow curve typically observed in PS in which a transition region appears instead of a second Newtonian region. The third type of flow curve was observed typically for SAN, which falls between the two types.

The molecular weight of such polymers as PS and SAN with strong molecular interaction decreases under high shear rates beyond the end of the first non-Newtonian region. On the other hand, only slight changes in molecular weight were observed for polymers with weak molecular interaction, such as HDPE.

A generalized flow curve was proposed to explain the observed flow behavior for the various polymers for a wide range of shear rates. According to the generalized flow curve, flow behavior is considered as follows.

In the first non-Newtonian region, viscosity depends on the entanglement density.

In the second Newtonian or transition region, the viscosity depends only on the friction of highly oriented molecules in which all the entanglements vanish and molecular scission occurs beyond a critical shear rate $\dot{\gamma}_c$.

In the second non-Newtonian region, the viscosity depends mainly on polymer scission.

The generalized flow curve adequately explains flow behavior in various polymers exposed to high shear rates.

The authors wish to express their thanks to Dr. O. Kamigaito, Toyota Central Research and Development Laboratories, Inc., for his discussion and encouragement. They should also like to thank Dr. Y. Kojima, Mr. K. Okabayashi, Mr. T. Ohmori, and Mr. Y. Ezaki for their assistance with some of the experimental works.

References

1. R. J. Crowson, A. J. Scott, and D. W. Saunders, *Polym. Eng. Sci.*, **21**, 748 (1981).
2. M. R. Kamal and H. Nyun, *Polym. Eng. Sci.*, **20**, 109 (1980).
3. D. C. Bogue, *Ind. Eng. Chem.*, **51**, 874 (1959).
4. L. D'Esposito and J. L. Koenig, *Polym. Eng. Sci.*, **19**, 162 (1979).
5. P. Fordyce and K. L. Devries, *Polym. Eng. Sci.*, **24**, 421 (1984).
6. R. S. Porter and J. F. Johnson, *Trans. Soc. Rheol.*, **6**, 107 (1962).
7. D. Soong and M. Shen, *Polym. Eng. Sci.*, **20**, 1177 (1980).

Received Febuary 6, 1985
Accepted March 22, 1985